ARTICLE

Biological Fabrication of Photoluminescent Nanocomb Structures by Metabolic Incorporation of Germanium into the Biosilica of the Diatom *Nitzschia frustulum*

Tian Qin,[†] Timothy Gutu,[‡] Jun Jiao,[‡] Chih-hung Chang,[†] and Gregory L. Rorrer[†,*]

[†]Department of Chemical Engineering, Oregon State University, Corvallis, Oregon 97331, and [‡]Department of Physics, Portland State University, Portland, Oregon 97207

ABSTRACT Diatoms are single-celled algae that make microscale silica shells or "frustules" with intricate nanoscale features such as two-dimensional pore arrays. In this study, the metabolic insertion of low levels of germanium into the frustule biosilica of the pennate diatom *Nitzschia frustulum* by a two-stage cultivation process induced the formation of frustules which strongly resembled double-sided nanocomb structures. The final product from the two-stage cultivation process contained 0.41 wt % Ge in biosilica and consisted of an equal mixture of parent frustule valves possessing a normal two-dimensional array of 200 nm pores and daughter valves possessing the nanocomb structure. The nanocomb structures had overall length of 8 μm, rib width of 200 nm, rib length of 500 nm, and slit width of 100 nm. Each slit of the nanocomb was most likely formed by a directed morphology change of a row of 200 nm pores to a single open slit following Ge incorporation into the developing frustule during the final cell division. The frustules possessed blue photoluminescence at peak wavelengths between 450 and 480 nm, which was attributed to contributions from nanostructured biosilica in both the parent valves and in the nanocomb daughter valves. This is the first reported study of using a cell culture system to biologically fabricate a photoluminescent nanocomb structure.

KEYWORDS: cell culture · diatoms · germanium · nanocomb · photoluminescence · silica

Currently, there is enormous interest in bioinspired processes for the fabrication and self-assembly of semiconductor nanostructures that possess unique optical and electronic properties.[1–5] Although biomimetic approaches typically focus on biomolecule-mediated processes, living cells also have the potential to direct the fabrication of nanostructured materials, particularly for photonic device applications.[6] In this regard, diatoms, a prolific class of single-celled algae that make microscale biosilica shells or "frustules" with intricate submicron features dominated by two-dimensional pore arrays, have been touted as a paradigm for the controlled production of nanostructured silica with interesting properties.[7]

The diatom *Nitzschia frustulum* possesses a frustule of ellipsoidal shape with bilateral symmetry, where linear arrays of ~200 nm pores span the top face of the frustule. Recently, we discovered that silica from bioreactor-cultured *N. frustulum* cells possessed blue photoluminescence, where the luminescence intensity and wavelength were dependent on the change in frustule nanostructure as the cell culture moved from the exponential to the stationary phase of growth.[8] Furthermore, we demonstrated that soluble germanium can be metabolically inserted into the biosilica of the pennate diatom *Pinnularia* sp. by a two-stage bioreactor cultivation process, where the incorporation of Ge into the frustule biosilica reduced the frustule pore diameter but otherwise did not affect the frustule morphology.[9]

In this paper, we report that the metabolic insertion of germanium into the frustule biosilica during cultivation of the diatom *Nitzschia frustulum* induced the fabrication of double-sided "nanocomb" frustule structures that possess blue photoluminescence. A nanocomb structure consists of nanoscale "teeth" or ribs joined together by a common backbone. To date, nanocomb structures have only been made of wurtzite semiconductor materials, principally ZnO, by thermal evaporation techniques.[10–14] ZnO nanocomb structures possess optoelectronic and piezoelectric properties which enable a variety of device applications.[15–18] ZnO structures can be replicated into silicon carbide,[19] but the fabrication of SiO_2 nanocombs has not been previously reported. Furthermore, there are

*Address correspondence to rorrergl@engr.orst.edu.

Received for review February 26, 2008 and accepted May 22, 2008.

Published online June 14, 2008.
10.1021/nn800114q CCC: $40.75

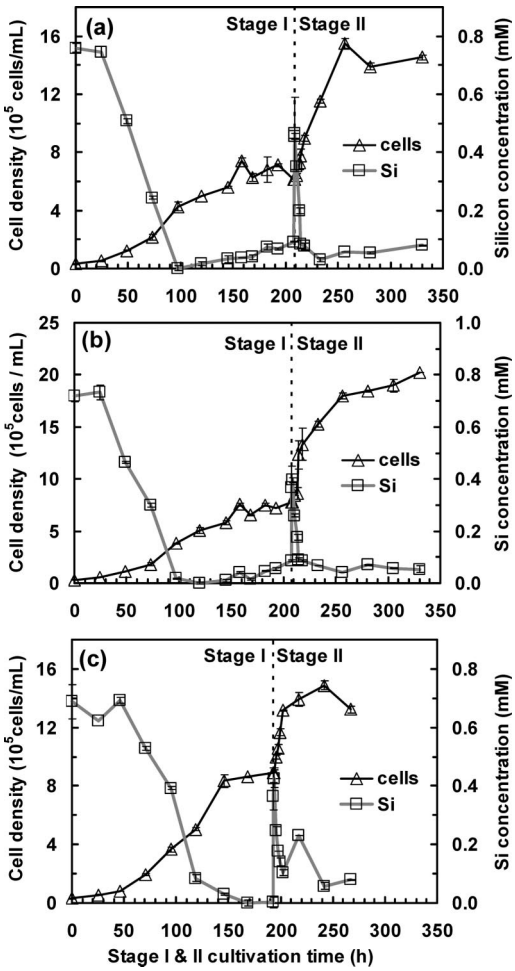

Figure 1. Two-stage diatom cell culture process for metabolic insertion of germanium into frustule biosilica of *N. frustulum*, detailing medium Si concentration and cell number density *versus* time: (a) 0.0 μM Ge initial Ge concentration in Stage II (control); (b) 6.7 μM initial Ge concentration in Stage II; (c) 23.0 μM initial Ge concentration in Stage II.

no reported studies of using bioinspired approaches to fabricate photoluminescent nanocomb structures.

Below, we describe a diatom cell cultivation process for the biological fabrication of biosilica nanocomb structures and their characterization by electron microscopy and photoluminescence spectroscopy.

RESULTS AND DISCUSSION

Two-Stage Bioreactor Cultivation. Cell number density and dissolved silicon (Si) concentration during the two-stage bioreactor cultivation of the diatom *N. frustulum* at two different initial concentrations (6.7 and 23 μM) of soluble germanium (Ge) in Stage II of the cultivation process are presented in Figure 1. For comparison, a representative control cultivation experiment where no Ge was added to Stage II of the cultivation process is also presented in Figure 1. The initial concentrations of Si and Ge in Stages I and II of the cultivation process were designed to control the final bulk concentration of Ge in the diatom biosilica. Details on Si and Ge delivery for each bioreactor experiment are provided in Table 1.

In Stage I of the cultivation process, an initial Si concentration of 0.70 mM without Ge coaddition resulted in nominally 4−5 cell doublings before all of the dissolved silicon was consumed. The concentration of soluble Si decreased commensurate with the increase in cell number density, and so substrate consumption was considered growth associated. When all of the soluble Si was consumed and the cell number density was constant for at least two photoperiods, the culture was considered to be in the silicon-starved state.

In Stage II of the cultivation process, a mixture of soluble Si and soluble Ge was fed to the silicon-starved diatom cell suspension. Dissolved Si and Ge concentrations in the culture suspension during Stage II of the cultivation process are compared in Figure 2 for two different initial concentrations of Ge (6.7 and 23 μM). The amount of silicon substrate added to Stage II of the cultivation process (0.4 mM) was designed to sustain only one more cell division. Both Si and Ge were rapidly taken up by the silicon-starved diatom cells within 10 h by a surge uptake mechanism,[9,20] which was accompanied by a doubling of the cell number density within 24 h after the initiation of Stage II. For the bioreactor cultivation at the higher initial Ge concentration of 23 μM, some efflux of Si from the cells back to the liquid culture medium was observed during Stage II. This efflux was commensurate with the dark phase of the photoperiod 10 h into Stage II. When illumination to the diatom culture resumed 20 h into Stage II during the light phase of the photoperiod, the residual dissolved silicon was consumed. Similar behavior was observed in our previous work during co-uptake of dissolved Si and Ge by the diatom *Pinnularia*.[8]

Process growth parameters are compared in Table 1 for different initial concentrations of soluble Ge in Stage II. The uptake of Ge by the diatom cells did not

TABLE 1. Process Parameters for Two-Stage Bioreactor Production of *N. frustulum* Biosilica Containing Metabolically Inserted Germanium

		initial germanium concentration in Stage II		
process parameter	stage	control	lowGe	highGe
		0.0 μM	6.7 ± 1.8 μM	23 ± 1 μM
initial silicon concn, $C_{Si,o}$ (mM)	I	0.72 ± 0.01	0.72 ± 0.02	0.69 ± 0.04
	II	0.47 ± 0.13	0.37 ± 0.08	0.36 ± 0.05
mol Si:Ge in feed	II		55:1	16:1
specific growth rate, μ (h^{-1})[a]	I	0.024 ± 0.002	0.024 ± 0.001	0.024 ± 0.001
	II	0.026 ± 0.003	0.027 ± 0.008	0.017 ± 0.005
cell number density, $X_{N,f}$ (10^6 cells/mL)	I	6.8 ± 0.4	7.3 ± 0.5	8.6 ± 0.4
	II	13.6 ± 2.0	18.9 ± 0.9	14.3 ± 0.9
cell yield, $Y_{Xn/Si}$ (10^9 cells/mmol Si)	I	9.2 ± 1.3	10 ± 1.0	12 ± 1.0
intracellular Ge (μmol Ge/g DW)[c]	II	~0	12 ± 1	28 ± 3
Inorganic solid (g SiO_2 /g DW)[b]	II	0.16 ± 0.07	0.13 ± 0.07	0.11 ± 0.06
bulk Ge content (wt % Ge in SiO_2)[c]	II	~0	0.14 ± 0.05	0.41 ± 0.13
nanocomb/parent valve ratio	II	0	1.1 ± 0.1	1.0 ± 0.1

[a]Stage I, exponential growth period 0−120 h (n = 6 data points); Stage II, exponential growth period 0−24 h (n = 6 data points). [b]Averaged 24−120 h Stage II, DW = dry biomass. [c]Stage II, 120 h.

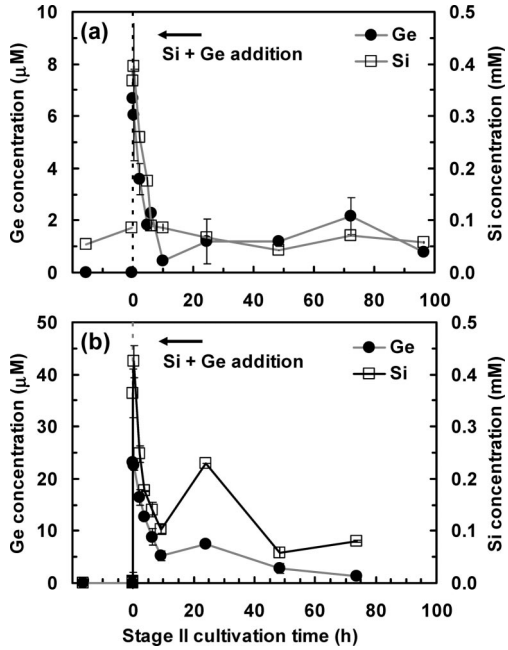

Figure 2. Two-stage diatom cell culture process for metabolic insertion of germanium into frustule biosilica of *N. frustulum*, detailing Ge and Si concentration *versus* time during Stage II: (a) 6.7 μM Ge initial Ge concentration in Stage II; (b) 23.0 μM initial Ge concentration in Stage II.

significantly affect the growth parameters. But at the highest initial Ge concentration, the growth rate (μ) decreased slightly, and the cell yield coefficient ($Y_{Xn/Si}$) increased, which means that the Si content per unit cell decreased. The concentrations of Ge in the hydrogen-peroxide-treated biosilica obtained from diatom cells at the end of Stage II of the bioreactor cultivation process are also presented in Table 1. After uptake of Ge, the diatom cells were thoroughly washed, and so only intracellular Ge was associated with the cell biomass. However, from material balance studies, only 21−22% of the intracellular Ge retained within the biomass was ultimately retained within the biosilica. Although hydrogen peroxide was effectively removed organic material, it is also known to etch Ge. Consequently, the Ge content in the biosilica reflected the metabolically inserted Ge that survived the hydrogen peroxide treatment step. The recovery of intracellular silicon after hydrogen peroxide treatment of the diatom cells was not determined.

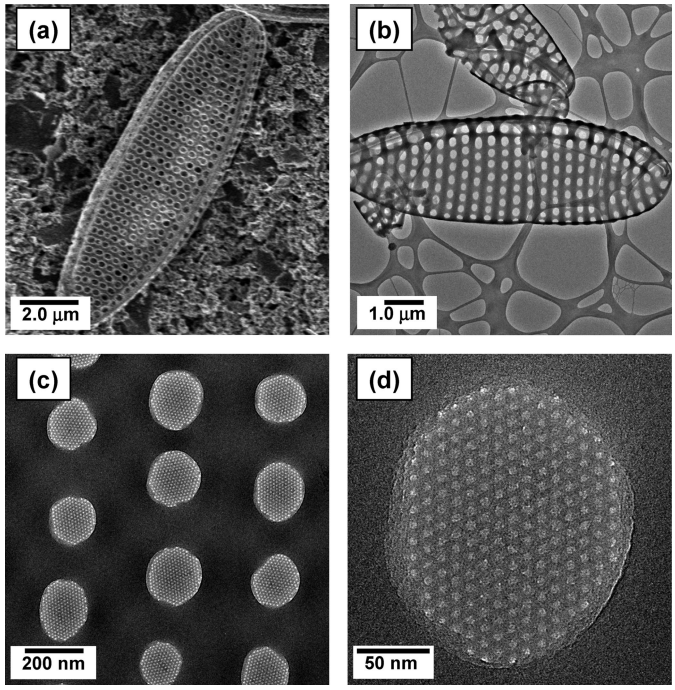

Figure 3. Electron microscopy images of *N. frustulum* biosilica at the end of Stage II, for the control experiment where no Ge was added. (a) SEM image of frustule, clearly showing raphae and fibula characteristic of Nitschoid symmetry; (b) TEM image of frustule; (c) TEM image of pore array; (d) TEM image of single pore, showing fine structures.

Electron Microscopy of Diatom Frustules with No Germanium. Electron microscopy images of the *N. frustulum* diatom frustules obtained from control cultivation experiments where germanium was not added to Stage II of the diatom suspension culture are presented in Figure 3. An SEM image of a representative frustule obtained at the stationary phase of Stage I of cultivation is presented in Figure 3a, whereas TEM images of a representative frustule at the end of Stage II of cultivation are presented in Figure 3b−d. As a pennate diatom, *N. frustulum* assumes an ellipsoidal shape of nominally 3 μm width (transverse axis) and 10 μm length (longitudinal axis). The frustule possesses upper and lower shells called theca that fit together like the halves of a Petri dish. The theca included a top face (valve) and a ring of pores around one side of the valve (fibulae structure). A solid strip of silica with a slit along its center (the raphae) defined the boundary between the valve and the fibulae structure. The valve microstructure consisted of a series of parallel rib structures aligned along the transverse axis. Between two parallel rib structures was a linear array of oval-shaped ~200 nm pores, also aligned along the transverse axis. The fibulae structure was wrapped around only one side the upper valve, and a separate fibulae structure was wrapped around the opposing side of the lower valve, a morphological feature known as Nitzschioid symmetry.[21]

At the end of Stage II of cultivation process, if no germanium was added to the diatom cell suspension, a secondary fine structure on the frustule valve was also observed. Specifically, a thin layer of nanostructured silica, most likely composed of a single layer of ~5 nm silica nanoparticles fused together in a hexagonal pattern, filled the base of each frustule pore, creating a secondary array of nanopores. The frustule biosilica surface also possessed a granular fine structure, which was also attributed to silica nanoparticles. Previous studies have also observed the frustule surface of other pennate diatoms is composed of nanoparticles.[22,23] This fine structure was only associated with stationary phase of growth after the last cell division, at the point of sili-

con starvation where both the dissolved silicon concentration in the medium was near zero and the cell density was constant for at least one photoperiod.

Electron Microscopy of Diatom Frustules Containing Germanium. Electron microscopy images of representative *N. frustulum* diatom frustule valves obtained from cultivation experiments where germanium was added to Stage II of the cultivation process at two different initial concentrations (6.7 and 23.0 μM) are presented in Figures 4–6. Isolation of biosilica frustules by aqueous hydrogen peroxide treatment of the diatom cells removed all organic materials from the diatom cells and separated the upper and lower theca, presumably by removing the girdle band proteins that bind the theca together. Therefore, by this isolation method, the valve structures could be imaged separately. Milder forms of the organic material removal from frustule biosilica, such as SDS detergent treatment, were not used in this study because they did not separate the upper and lower theca.

At the end of Stage II of the cultivation process, two valve structures were identified. To facilitate the interpretation of TEM images representing these structures, Figure 7 schematically represents the valve structure of the diatom frustule after metabolic insertion of germanium into the biosilica. During Stage II of cultivation, enough soluble silicon was added to the culture suspension to enable all of the silicon-starved cells from Stage I of cultivation to undergo one more cell division. Therefore, each new diatom cell possessed a parent valve from Stage I of cultivation, and a new daughter valve formed during Stage II of cultivation of altered morphology that contained germanium imbedded within its frustule biosilica.

Figure 4 presents TEM images of representative parent and daughter frustule valves obtained from the end of Stage II of the cultivation experiment where 6.7 μM Ge was added to the culture at the beginning of Stage II. The bulk germanium concentration in the frustule biosilica, which represented the average of the parent and daughter valves, was at the low Ge level of 0.141 ± 0.046 wt % in SiO_2 (Table 1). The parent frustule valve possessed the intact frustule pore array, but nanoparticles littered the frustule surface and partially filled the frustule pores (Figure 4a−c). In contrast, the new (daughter) frustule valve formed after Ge addition to the diatom cell suspension culture consisted of a parallel array of nanoscale ribs fixed to a common backbone (Figure 4d−f), where the backbone was derived from the fusion of the raphae and fibulae structures. Apparently, to form this structure, each linear array of pores running along the transverse axis of the frustule was now just a single open slit. Lining the base of each open slit was a layer of ~3−5 nm nanoparticles. This nanoparticle layer was only found in an area where a pore would have formed. The nanoslit arrays were

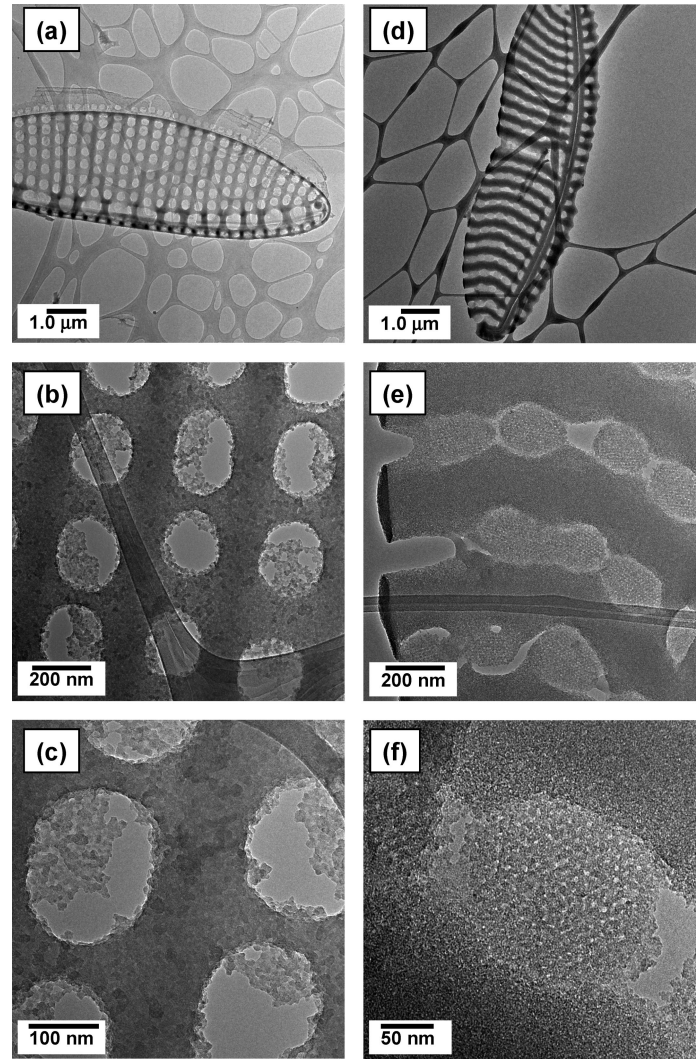

Figure 4. TEM images of *N. frustulum* valves at the end of Stage II, for the cultivation experiment carried out at a 6.7 μM initial concentration of Ge in Stage II. The bulk Ge concentration was 0.14 wt % in the frustule biosilica. (a−c) Parent valve, showing intact pore structure with nanoparticles littering the surface; (d−f) daughter valve of nanocomb morphology, showing nanoparticles lining the base of each slit.

slightly curved along the transverse axis. These features were consistent with "nanocomb" structures.

Presented in Figures 5 and 6 are TEM images of representative frustules obtained from the end of Stage II of the cultivation experiment where 23 μM Ge was added to the culture (Table 1). The bulk germanium concentration in the frustule biosilica, which represented the average of the parent and daughter valves, was at the high Ge level of 0.411 ± 0.129 wt % in SiO_2. Figure 5 reveals the fine structure of the parent frustule with the intact pore structure, whereas Figure 6 details the fine structure of the morphologically altered daughter frustule. Although the surfaces of both the parent and daughter frustule valves had a granular texture, nanoparticles did not litter the frustule surface or fill the frustule pores.

Figure 6 presents three representative nanocomb structures characteristic of the new daughter valve. At

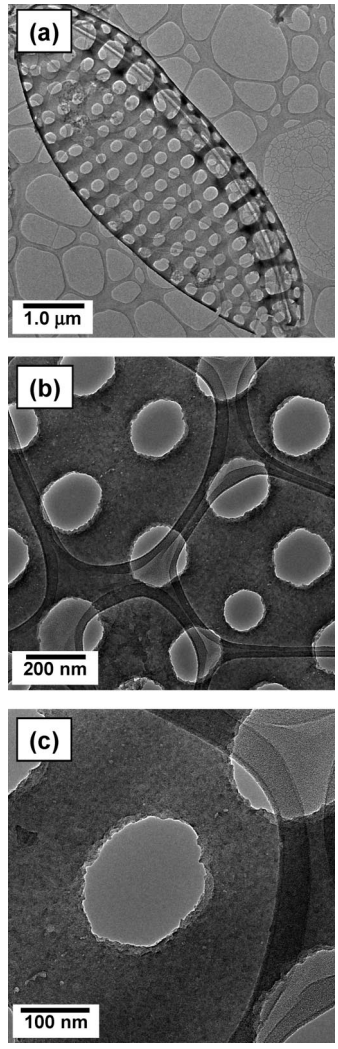

Figure 5. TEM images of *N. frustulum* "parent valves" at the end of Stage II, for the cultivation experiment carried out at a 23.0 μM initial concentration of Ge in Stage II: (a) valve; (b) pore array; (c) single pore detail.

the higher bulk Ge concentration in the biosilica, the rib structures were nominally straight, with a rib width of 200 nm, open slit width of 100 nm, slit-to-slit spacing of 300 nm, and rib length ranging from about 500 nm to 1.5 μm. Furthermore, a second array of shorter nanoscale ribs, formed from residual fibulae structure, was also formed. No nanoparticles were observed lining the base of the slit. A STEM-EDS elemental line scan analysis of a representative nanoslit array is presented in Figure 8, where the final bulk germanium concentration in the frustule biosilica was 0.41 wt %. Germanium was uniformly distributed into the frustule biosilica of the nanocomb array. STEM-EDS spot analysis of a representative parent valve showed only Si and O in the atomic proportion of SiO_2.

The ratio of parent valve structures to the new daughter valve nanocomb structures was approximately 1:1, based on enumeration of each structure type from 20 SEM images per sample (Table 1). We have showed in previous studies[9,20] that Ge uptake only occurs concurrently with Si uptake in Stage II of the cultivation process. Consequently, when the Si uptake was sufficient for cell division, the each new valve that was formed contained Ge. This process was limited to one cell doubling, as the new cell containing one aberrant nanocomb structure was not likely to divide again. Under these simplifying assumptions, the ratio of parent valves to daughter nanocomb valves can also be estimated from bioreactor cultivation data by the relationship

$$\frac{X^{D}_{N,II}}{X^{P}_{N}} = \frac{X_{N,f} - X_{N,o}}{X_{N,o}} \quad (1)$$

where X^{P}_{N} is the number density of parent valves, $X^{D}_{N,II}$ is the number density of daughter nanocombs valves generated by Stage II of cultivation, and $X_{N,o}$ and $X_{N,f}$ are the initial and final cell densities of Stage II of cultivation. Equation 1 predictions reasonably matched the experimentally determined values enumerated from SEM images. No attempt was made to isolate the nanocombs from the parent frustule valves.

Role of Germanium in Formation of Diatom Nanocomb Structures. The addition of a mixture of soluble silicon and germanium to silicon-starved *N. frustulum* diatom cells and the subsequent metabolic insertion of germanium into the biosilica during frustule development induced the formation of the nanocomb structures. In the living diatom cell, biosilica frustule development is a bottom-up fabrication process that proceeds by a complex series of biochemical and cellular events during the cell division cycle.[24] The three major processes are (1) uptake of soluble $Si(OH)_4$ into the cell by silicon transporter proteins imbedded in the cell membrane,[25] (2) "silaffin" protein-mediated condensation of soluble $Si(OH)_4$ to nanostructured silica, *e.g.*, silica nanoparticles, within the silica deposition vesicle (SDV), and (3) patterning of nanostructured silica within the SDV by phase-partitioning processes that leads to the formation of the ordered pore arrays.[7] Imbedded within these processes are the biochemical and cellular events that mediate the formation and molding of the silica deposition vesicle itself at the plane of cell division. Subtle variations in SDV development and biosilica deposition lead to the myriad of diatom frustule fine structures that can be fabricated through this common metabolic theme.[26,27]

Silicon is a required substrate for diatom cell division. When the cell is in the silicon starved state, the cell takes up a mixture of both soluble $Si(OH)_4$ and $Ge(OH)_4$, and then incorporates the Ge into the frustule biosilica. This process induced a directed change in frustule morphology that occurred at low levels of Ge incorporation into the frustule biosilica. The biochemical and cellular mechanisms underlying the change in valve morphology of *N. frustulum* from a pore array to a

nanocomb array can only be speculated upon at this point. If $Ge(OH)_4$ was only inserted into the frustule biosilica during $Si(OH)_4$ condensation to SiO_2, then putative Ge−O−Ge and Si−O−Ge structures would possess a bond angle and unit cell size different than Si−O−Si structures. Detailed material characterization of the Ge-imbedded biosilica was not attempted in this study because of the low level of Ge in the frustule biosilica and the amorphous character of the biogenic material. However, it is reasonable to expect that these defects could disrupt the complex processes of biosilica valve assembly. In pennate diatoms, valve assembly begins with the formation of the rib structures; silica then fills in between the ribs in a way that forms the pore array.[21] In *N. frustulum*, metabolic insertion of germanium most likely attenuated the rib formation step and eliminated the pore formation step, fortuitously leading to formation of the nanocomb array.

Previously, we showed that incorporation of 0.2−1.0 wt % Ge into the frustule biosilica of the pennate diatom *Pinnularia* reduced the frustule pore diameter and thickened the frustule, but the pores did not fuse together.[9] *Pinnularia* valves possess a central raphae which is aligned along the longitudinal axis of symmetry. The rib structures grow symmetrically from each side of the raphae to the edge of the valve.[28] In contrast, for *N. frustulum,* the raphae systems of the two valves lie on opposite sides along the valve edge. Consequently, the "Nitzschioid symmetry"[21] of *N. frustulum* was exploited to produce the asymmetric double-sided nanocomb structure of the new frustule valve following metabolic insertion of germanium.

There are limited previous studies on the effects of metal ions on frustule development during diatom cell culture, and none have demonstrated the directed fabrication of nanocomb structures. Recently, Townley *et al.*[29] reported that the pore diameter of frustules isolated from the centric diatom *Coscinodiscus wailesii* increased when the cells were grown in the presence of 3 μM nickel sulfate. Earlier, *Nitzschia lieberthrutti* diatom cells grown in the presence of 1.5 μg L^{-1} of Hg^{2+} or Sn^{2+} ions produced valves that possessed a lower length/diameter ratio,[30] whereas various pennate diatoms grown in the presence of Ge produced disordered and thickened valve structures.[31]

Biosilica nanocombs fabricated through *N. frustulum* cell culture have many morphological features in common with double-sided ZnO nanocombs.[14] However, these double-sided nanocombs were symmetric, whereas the biologically fabricated nanocombs described in this study were asymmetric, as they reflected the frustule morphology of the organism. To date, only wurtzite structured semiconductors, particularly ZnO, have been demonstrated to form nanocomb structures when synthesized by a high-temperature, solid−vapor phase thermal evaporation technique.[10–13] ZnO nanocomb structures possess photoluminescence[11,12] and have potential applications as diffraction gratings,[15] ultraviolet laser arrays,[16] gas sensors,[17] and biosensors.[18]

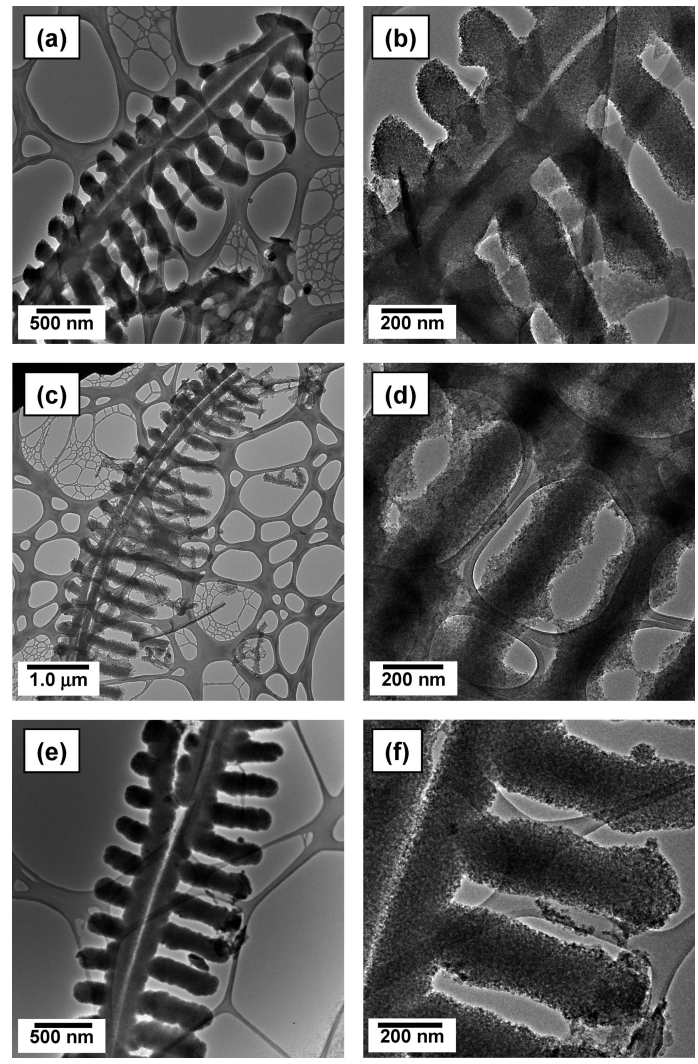

Figure 6. TEM images of *N. frustulum* "daughter valves" at the end of Stage II, for the cultivation experiment carried out at 23 μM initial concentration of Ge in Stage II. The bulk Ge concentration was 0.41% in the frustule biosilica. (a−c) Three representative nanocomb structures, showing range of variability in morphology; (d−f) fine structure of each nanocomb.

Photoluminescence of Diatom Nanocombs. Like ZnO nanocombs, diatom biosilica nanocombs also possess photoluminescence. A representative photoluminescence (PL) spectrum of *N. frustulum* biosilica sample containing 0.411 ± 0.129 wt % in SiO_2 is presented in Figure 9a. A comparison of the peak PL intensity for biosilica containing no Ge (control), 0.141 ± 0.046 wt % Ge, and 0.411 ± 0.129 wt % is presented in Figure 9b. Details on the cultivation history for each sample are provided in Table 1. Averaged results from samples obtained at 72, 96, and 120 h into Stage II are reported. All samples possessed blue or blue-green photoluminescence at peak wavelengths ranging from 450 to 480 nm, but there was no statistically significant difference in the peak PL intensity.

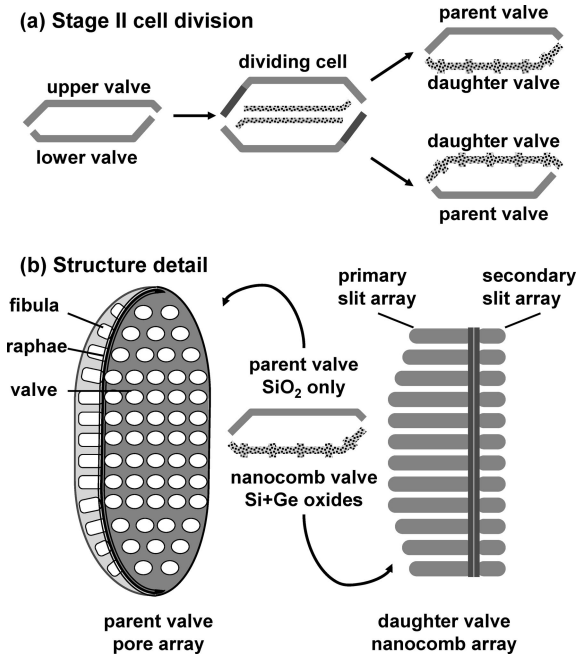

Figure 7. Schematic of diatom frustule obtained at the end of Stage II of cultivation: (a) cell division during Stage II; (b) structures of the parent valve and the daughter valve.

In a previous study, we showed that nanostructured silica obtained from cultivation of the diatom *N. frustulum* possessed blue photoluminescence, where

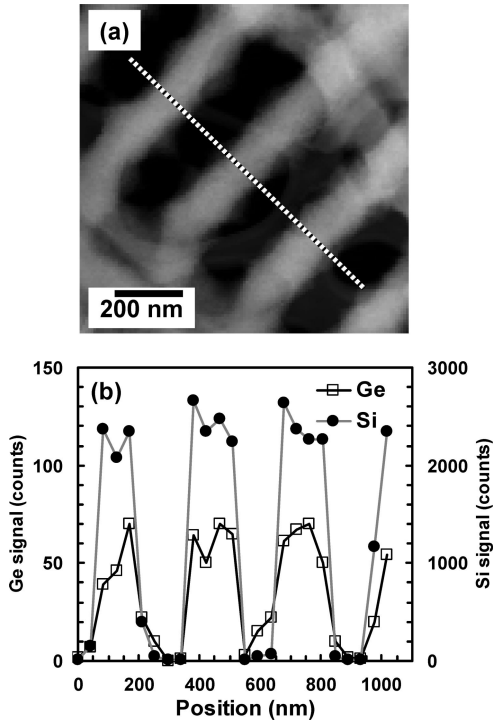

Figure 8. STEM-EDS profiling of fine structure from a *N. frustulum* daughter valve at the end of Stage II, for the cultivation experiment carried out at 23 μM initial concentration of Ge in Stage II. The bulk Ge concentration was 0.41% in the frustule biosilica. (a) Brightfield STEM image of nanoslit array, showing path of elemental line scan; (b) relative Si and Ge abundance along line scan, based on Kα signals for Si (1.74 keV) and Ge (9.86 keV, $K\alpha_1$).

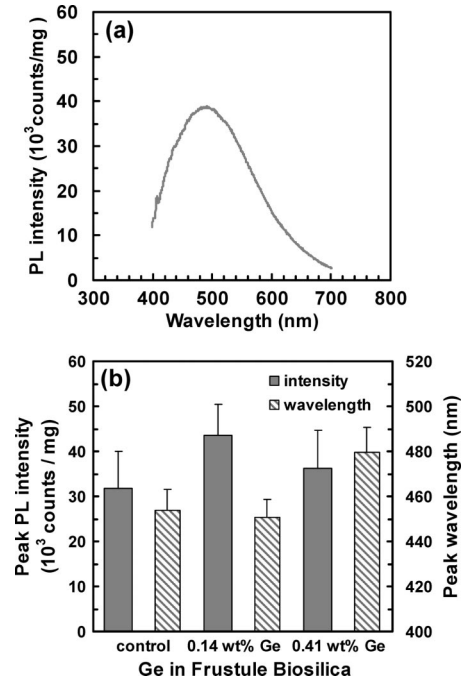

Figure 9. Photoluminescence (PL) of *N. frustulum* biosilica. (a) PL spectra from biosilica containing 0.41 wt % Ge; (b) comparison of peak PL intensity and wavelength for biosilica obtained from the control experiment (no Ge in Stage II, 0.0 wt % Ge), low Ge incorporation experiment (0.14 wt % Ge), and high Ge incorporation experiment (0.41 wt % Ge).

the PL emission likely most originated from surface defect sites associated with the nanostructured biosilica, particularly the nanoparticle assemblies constituting the solid biosilica.[8] In this present study, the metabolic insertion of small amounts (0.41 wt % Ge) into the frustule biosilica did not affect the gross PL intensity of the final biosilica obtained from Stage II of the cultivation process. The gross PL intensity would represent the sum of PL contributions from the parent valve and daughter valve nanocomb structures in the sample. Consequently, since the PL intensity of the bulk sample did not decrease, and the nanocomb structures represented at least 50% of the total frustule count (Table 1), then the nanocomb structures in the mixture must also be photoluminescent. Furthermore, the presence of nanocomb structures did not significantly alter the PL spectra shape or peak wavelength. Therefore, the intrinsic PL from the both nanocomb structure of the daughter valve and the two-dimensional pore structure of the parent valve most likely originated from the same source, the nanoparticle assemblies which constituted the solid biosilica of each structure.

SUMMARY

In this study, we harnessed the cellular biomineralization processes of living diatom cells to fabricate microscale shells (frustules) of biogenic silica that strongly resembled double-sided nanocomb structures. The biosilica nanocombs possessed blue photoluminescence. A

two-stage bioreactor cultivation process provided germanium to the diatom cells, and metabolic insertion of germanium into the frustule biosilica induced the formation of the nanocomb structure. The biological processes responsible for the fabrication of the nanocomb structure and the likely origins of its photoluminescence were discussed. The bioreactor cultivation process was carried out at ambient conditions, used environmentally benign source materials, and fabricated the nanocombs by a bottom-up self-assembly process on a massively parallel scale. This study provides a unique example of how cell culture systems can be externally directed to fabricate interesting nano- and microstructured inorganic materials with optoelectronic properties.

MATERIALS AND METHODS

Bioreactor Cultivation of *Nitzschia frustulum*. Pure cultures of the photosynthetic marine diatom *Nitzschia frustulum* were obtained from the UTEX Culture Collection of Algae (UTEX # 2042) and maintained on seawater medium supplemented with inorganic nutrients.[20] The diatom cell suspension was cultivated under controlled conditions of light, pH, CO_2 delivery, and nutrient delivery using a bubble-column photobioreactor described previously.[9] Bioreactor cultivations were carried out at 150 $\mu E\ m^2\ s^{-1}$ incident light intensity, 14 h light/10 h dark photoperiod, 0.71 L air L culture^{-1} min^{-1} aeration rate (~350 ppm CO_2), and constant temperature of 22 °C.

The bioreactor cultivation process was carried out in two stages. In Stage I of the cultivation process, the bioreactor culture was inoculated to initial cell number density of $\sim 3 \times 10^5$ cells/mL from flask-cultured *N. frustulum* diatoms harvested at the stationary phase of growth. Soluble silicon was added to the diatom suspension as Na_2SiO_3 to initial concentration of 0.70 mM, which was sufficient to support at least four cell doublings. The culture was considered silicon starved when all of the soluble silicon was consumed and the cell number density was constant for at least two photoperiods. In Stage II of the cultivation process, a mixture of soluble Na_2SiO_3 and soluble GeO_2 was added to the silicon-starved diatom cell suspension 4 h into the light phase of the photoperiod. The total duration of Stage II was 120 h. The initial nitrate and phosphate concentrations in the bioreactor cultivation medium were 8.0 and 0.40 mM, respectively, to eliminate the possibility of macronutrient limited growth during both Stages I and II. The average pH of the culture suspension during Stage II ranged from 8.4 to 8.9. The time course of the two-stage bioreactor cultivation process was followed by measurements of cell number density, silicon concentration, and germanium concentration as described previously.[9] The specific growth rate was estimated from the least-squares slope of the linear portion of the cell density *versus* cultivation time data on a semilog plot. For Stage I, the linear region of the growth curve on a semilog plot was 0−120 h, whereas for Stage II, the linear region was only 0−24 h because only one cell division was allowed.

Frustule Biosilica Isolation and Ge Analysis. Details of all frustule biosilica isolation and Ge analysis procedures are previously described.[9] At the end of Stage II, the *N. frustulum* diatom cells were treated with 30 wt % aqueous hydrogen peroxide at pH 2.5 to remove the organic materials and isolate the intact biosilica frustule. Typical recoveries ranged from 0.11−0.16 g of inorganic solid/g dry cell mass. Aqueous hydrogen peroxide treatment also etched out some of the germanium oxides associated with the frustule biosilica. The frustule biosilica was analyzed for bulk germanium content by ion-coupled plasma (ICP) elemental analysis.

Electron Microscopy. Details of all electron microscopy procedures were previously described.[9] For transmission electron microscopy (TEM), diatom frustules were dispersed in methanol, deposited on a holey carbon copper grid, and then imaged by a FEI Tecnai F20 high-resolution TEM (200 keV) equipped with an embedded scanning transmission electron microscopy (STEM) mode and an X-ray energy dispersive analysis (EDS) probe. For scanning electron microscopy (SEM), diatom frustules dispersed in methanol were pipetted onto carbon tape, and allowed to dry, and then imaged without sample coating by a FEI Sirion field emission SEM at 2.0 keV. Two different types of frustule valve morphologies—parent valves *versus* daughter nanocomb valves—were enumerated from SEM images taken at ~2500×. Intact frustule structures were counted from a 4 × 5 grid of 20 images (~200 total structures) and statistically analyzed.

Photoluminescence (PL) Spectroscopy. Details of the photoluminescence measurements were previously described.[8] The PL spectrum of diatom frustule powder isolated by hydrogen peroxide treatment of cultured diatom cells was obtained at room temperature using a 337 nm N_2 laser excitation source.

Acknowledgment. This research was supported by the National Science Foundation (NSF) under Nanoscale Interdisciplinary Research Team (NIRT) award number BES-0400648.

REFERENCES AND NOTES

1. Dujardin, E.; Mann, S. Bio-Inspired Materials Chemistry. *Adv. Mater.* **2002**, *14*, 1–14.
2. Sarikaya, M.; Tamerler, C.; Jen, A. K. Y.; Schulten, K.; Baneyx, F. Materials Assembly and Formation Using Engineered Polypeptides. *Nat. Mater.* **2003**, *2*, 577–585.
3. Zhang, S. Fabrication of Novel Biomaterials through Molecular Self Assembly. *Nat. Biotechnol.* **2003**, *21*, 1171–1178.
4. Depero, L. E.; Curri, M. L. Inorganic Self Assembly. *Curr. Opin. Solid State Mater.* **2004**, *8*, 103–109.
5. Lagziel-Simis, S.; Cohen-Hadar, N.; Moscovich-Dagan, H.; Wine, Y.; Freeman, A. Protein Mediated Nanoscale Biotemplating. *Curr. Opin. Biotechnol.* **2006**, *17*, 569–573.
6. Parker, A. R.; Townley, H. E. Biomimetics of Photonic Nanostructures. *Nat. Nanotechnol.* **2007**, *2*, 347–353.
7. Sumper, M.; Brunner, E. Learning From Diatoms: Nature's Tools for the Production of Nanostructured Silica. *Adv. Funct. Mater.* **2006**, *16*, 17–26.
8. Qin, T.; Gutu, T; Jiao, J.; Chang, C.-H.; Rorrer, G. L. Photoluminescence of Silica Nanostructures from Bioreactor Culture of Marine Diatom *Nitzschia frustulum*. *J. Nanosci. Nanotechnol.* **2008**, *8*, 2392–2398.
9. Jeffryes, C.; Gutu, T.; Jiao, J.; Rorrer, G. L. Two-Stage Photobioreactor Process for the Metabolic Insertion of Nanostructured Germanium into the Silica Microstructure of the Diatom *Pinnularia* sp. *Mater. Sci. Eng. C* **2008**, *28*, 107–118.
10. Ma, C.; Moore, D.; Li, J.; Wang, Z. L. Nanobelts, Nanocombs, and Nanowindmills of Wurtzite ZnS. *Adv. Mater.* **2003**, *15*, 228–231.
11. Wang, Z. L. Zinc Oxide Nanostructures: Growth, Properties, and Applications. *J. Phys.: Condens. Matter* **2004**, *16*, R829−R858.
12. Wang, Z. L. Novel Nanostructures of ZnO for Nanoscale Photonics, Optoelectronics, Piezoelectricity, and Sensing. *Appl. Phys. A: Mater. Sci. Process.* **2007**, *88*, 7–15.
13. Lao, J. Y.; Huang, J. Y.; Wang, D. Z.; Ren, Z. F. Hierarchical Oxide Nanostructures. *J. Mater. Chem.* **2004**, *14*, 770–773.
14. Lao, C. S.; Gao, P. X.; Yang, R. S.; Zhang, Y.; Dai, Y.; Wang, Z. L. Formation of Double-Teethed Nanocombs of ZnO and Self-Catalysis of Zn-Terminated Polar Surface. *Chem. Phys. Lett.* **2006**, *417*, 358–362.
15. Pan, Z. W.; Mahurin, S. M.; Dai, S.; Lowndes, D. H. Nanowire Array Gratings with ZnO Combs. *Nano Lett.* **2005**, *5*, 723–727.
16. Yan, H.; He, R.; Johnson, J.; Law, M.; Saykally, R. J.; Yang, P. Dendritic Nanowire Ultraviolet Laser Array. *J. Am. Chem. Soc.* **2003**, *125*, 4728–4729.

17. Comini, E.; Faglia, G.; Ferroni, M.; Sberveglieri, G. Gas Sensing Properties of Zinc Oxide Nanostructures Prepared by Thermal Evaporation. *Appl. Phys. A.* **2007**, *88*, 45–48.
18. Wang, J. X.; Sun, X. W.; Wei, A.; Lei, Y; Cai, P.; Li, C. M.; Dong, Z. L. Zinc Oxide Nanocomb Biosensor for Glucose Detection. *Appl. Phys. Lett.* **2006**, *88*, 233106.
19. Zhou, J; Liu, J.; Yang, R.; Lao, C.; Gao, P.; Tummala, R.; Xu, N.-S.; Wang, Z. L. SiC-Shell Nanostructures Fabricated by Replicating ZnO Nano-objects: A Technique for Producing Hollow Nanostructures of Desired Shape. *Small* **2006**, *2*, 1344–1347.
20. Rorrer, G. L.; Chang, C.-H.; Liu, S.-H.; Jeffryes, C.; Jiao, J.; Hedberg, J. A. Biosynthesis of Silicon-Germanium Oxide Nanocomposites by Marine Diatoms. *J. Nanosci. Nanotechnol.* **2005**, *5*, 41–49.
21. Round, F. E.; Crawford, R. M.; Mann, D. G. *The Diatoms*; Cambridge University Press: Cambridge, 1990.
22. Crawford, S. A.; Higgins, M. J.; Mulvaney, P.; Wetherbee, R. Nanostructure of the Diatom Frustule as Revealed by Atomic Force and Scanning Electron Microscopy. *J. Phycol.* **2001**, *37*, 543–554.
23. Noll, F.; Sumper, M.; Hampp, N. Nanostructure of Diatom Silica Surfaces and of Biomimetic Analogues. *Nano Lett.* **2002**, *2*, 91–95.
24. Martin-Jézéquel, V; Hildebrand, M.; Brzeziniski, M. A. Silicon Metabolism in Diatoms: Implications for Growth. *J. Phycol.* **2000**, *36*, 821–840.
25. Thamatrakoln, K.; Alverson, A. J.; Hildebrand, M. Comparative Sequence Analysis of Diatom Silicon Transporters: Toward a Mechanic Model for Silicon Transport. *J. Phycol.* **2006**, *42*, 822–834.
26. Mann, S. The Chemistry of Form. *Angew. Chem., Int. Ed.* **2000**, *39*, 3392–3406.
27. Zurzolo, C.; Bowler, C. Exploring Bioinorganic Pattern Formation in Diatoms. A Story of Polarized Trafficking. *Plant Physiol.* **2001**, *127*, 1339–1345.
28. Pickett-Heaps, J. D.; Tippit, D. H.; Andreozzi, J. A. Cell Division in the Pennate Diatom Pinnularia. III - The Valve and Associated Cytoplasmic Organelles. *Biol. Cellulaire* **1979**, *35*, 195–205.
29. Townley, H. E.; Woon, K. L.; Payne, F. P.; White-Cooper, H.; Parker, A. R. Modification of the Physical and Optical Properties of the Frustule of the Diatom *Coscinodiscus wailesii* by Nickel Sulfate. *Nanotechnology* **2007**, *18*, 295101.
30. Saboski, E. M. Effects of Mercury and Tin on the Ultrastructure of the Marine Diatom *Nitzschia liebethrutti*. *Water Air Soil Poll.* **1977**, *8*, 461–466.
31. Chiappino, M. L.; Azam, F.; Volcani, B. E. Effect of Germanic Acid on Developing Cell Walls of Diatoms. *Protoplasma* **1977**, *93*, 191–204.